High-Performance Electric Two-Wheeler Fast Charger Based on Intelligent Control Algorithm

Submitted: 26th August 2024; accepted: 17th February 2025

Subiyanto, Rizky Ajie Aprilianto, Mario Norman Syah, Bagaskoro Saputro, Abdurrakhman Hamid Al-Azhari, Nektar Cahayasabda, Bayu Adi Pambudi, Faiq Mananul Faqih, Icha Arifah Annisa, Dwi Bagas Nugroho, Siva Khaaifina Rachmat, Dewi Anggriani

DOI: 10.14313/jamris-2026-030

Abstract:
Conventional electric two-wheeler (E2W) chargers suffer from prolonged charging times and battery nonlinear characteristics, limiting user flexibility and compliance with evolving battery standards. This work developed a high-performance fast charger utilizing an interleaved buck converter (IBC) governed by a hybrid proportional integral–fuzzy logic control (PI-FLC) algorithm. The PI-FLC dynamically optimizes charging current/voltage by integrating real-time battery current, voltage, and state-of-charge (SoC) data. The IBC architecture minimizes output current ripple, enabling compact filter design. The hybrid algorithm maintains a particular voltage and current threshold, ensuring compliance with E2W battery characteristics. The proposed system achieves 0–100% SoC in 57.75 minutes—a 67.9% and 75.9% reduction compared to PID CC-CV (180 min) and PI-CV (240 min), respectively. Moreover, the proposed method outperforms several cutting-edge charging methods, such as a Zeta converter with sliding mode control (SMC) (98.1% efficiency, 80 min), Quasi-Resonant converters with hysteresis control (97.5%, 70 min), Interleaved Boost with FLC (98.5%, 65 min), and Dual Active Bridge with MPC (97.9%, 75 min). Furthermore, hardware implementation demonstrated 98.8% efficiency at 0.22 C-rate and empirically validated charger compatibility across E2W battery topologies. This work bridges the gap between rapid charging demands and battery longevity, offering a scalable solution for next-generation E2W ecosystems.

Keywords: *electric two-wheelers (E2W), fast charger, interleaved buck converter (IBC), proportional integral–fuzzy logic control (PI-FLC)*

1. Introduction

The petroleum transition as the primary energy source for the transportation sector has been a crucial issue. It is conducted as a response to escalating concerns regarding climate change [1]. Decarbonizing by adopting electric vehicles (EVs) is an environmentally sustainable and practical solution [2]. It is becoming increasingly popular worldwide, heralding a new era of automotive sustainability. Concurrently, initiatives in renewable energy systems are being implemented globally [3]. Hence, the development of EV technology has been massively conducted to result in superior performance.

As a part of EV development, electric two-wheelers (E2Ws), including electric bicycles/electric motorcycles [4], emerge as the preferable alternative for countries such as Indonesia due to the socio-economic conditions and the existing transportation infrastructure. More than 2000 EVs passed the feasibility test in 2020 by the Directorate General of Land Transportation Indonesia, and the E2Ws are the highest unit among others [5]. In addition, the sales of E2Ws are higher than those of other EV types.

The application of E2Ws is intrinsically linked to using batteries as an energy storage medium. Batteries are designed to be rechargeable, necessitating appropriate charging devices [6]. EV charging duration is influenced by battery capacity, charger power, and battery technology, where larger batteries take longer, high-power chargers speed up charging, and charging efficiency depends on the power converter [7]. Choosing a converter topology and a suitable charging method are critical considerations in obtaining an appropriate charging device. The technology selection refers to the power converter topology, which has the capability of converting and conducting power optimally. Various control techniques have been developed to enhance the efficiency and stability of E2Ws DC-DC converters, such as Voltage Mode Control (VMC), Current Mode Control (CMC), PID, Sliding Mode Control (SMC), and Fuzzy Logic Control (FLC)[8].

Converter efficiency is a primary parameter in power conversion systems that measures the ratio between the obtained output power and the input power used. According to [9], high-efficiency converters can reduce power losses and improve the overall performance of the power system. In [10] it was added that converter efficiency is inversely proportional to the total power loss in the converter, making it a key factor in designing optimal electrical power systems. Furthermore, [11] explained that increasing converter efficiency can be achieved by optimizing circuit topology and reducing parasitic resistance in power components. Meanwhile, the most prevalent strategy for recharging batteries has been adopted, which is constant current–constant voltage (CC-CV).

Power converters play a critical role in modifying, controlling, and conditioning electrical power within power systems by adjusting voltage levels. This adjustment can take the form of increasing (boost) or decreasing (buck) voltage or a combination of both (buck-boost) [12]. Recent research, highlighted in [13], introduces a current-fed non-isolated DC–DC converter design that employs fewer switching components and utilizes Zero Voltage Switching (ZVS) and Zero Current Switching (ZCS) techniques to mitigate power losses. This methodology incorporates a Coati-optimized Fractional Order Proportional-Integral-Derivative (FOPID) controller. However, it still encounters challenges, including switch voltage stress and limited adaptability to various battery types, indicating a need for further optimization.

Additionally, [14] presents a bidirectional DC–DC converter utilizing Fractional Order Resonant (FOPR) control in conjunction with ZVS–ZCS techniques. This combination yields high efficiency, reduces power loss, and enhances stability. However, it faces ongoing challenges related to practical implementation and experimental validation. Addressing those shortcomings, previous studies have focused on developing fast-charging strategies, such as [15] proposed design of an electric bike charger based on a CUK converter operating in discontinuous conduction mode (DCM) CC–CV charging solution capable of charging 0-100% SoC of a 48 V, 20 Ah battery 2 hours. However, only batteries with certain specifications can accept DCM conditions. In [16], the design and implementation of a battery charger utilize SoC estimation and FLC charging. However, this method also requires around 1.5 hours to recharge 0-100% of the SoC battery to get the appropriate power for battery charging topology. [17] presents an ANFIS-based charging algorithm to increase charging speed. The complexity of ANFIS-based chargers is unreliable to conventional users because they potentially increase the charging price.

Furthermore, available conventional E2W chargers take approximately 2-9 hours to recharge 0-100% of their capacity. It is necessary that the charging time be faster to fulfil the user's high mobility and be safe and reliable by considering the battery's charging current capacity. Previous studies, such as in [16–18] have presented a suitable method for fast charging but still need to consider the specifications and capacity of the batteries on the market.

This study introduces a novel intelligent fast charger for E2Ws, utilizing a three-phase interleaved synchronous buck converter (3Phase IBC) for efficient power conversion and rapid, safe charging. The system is controlled by a proportional integral-fuzzy logic control (PI-FLC) algorithm.

2. E2W Charging Architecture

Figure 1 illustrates the selected charger topology suitable for various E2W devices. The selected universal off-board charging topology, as shown in Fig. 2, comprises a linear transformer, AC–DC converter, and

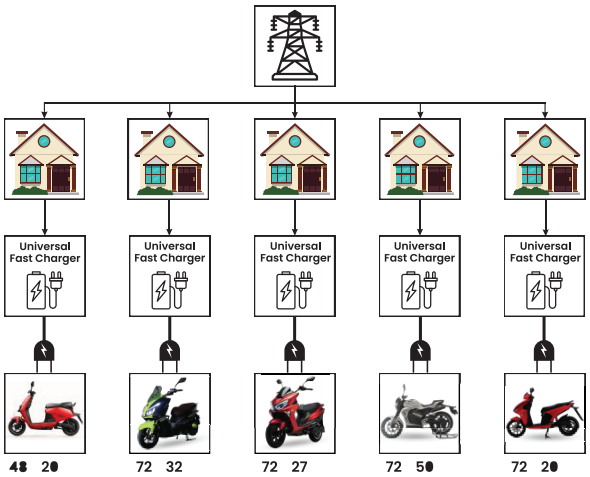

Figure 1. Charger application

DC–DC converter. The three-phase interleaved DC–DC converter is designed in a continuous current mode (CCM) where each switching device phase is shifted to 120° in accordance with the duty cycle $d_t(s)$ generated using the fuzzy logic algorithm. For configurations involving a greater number of phases, the phase shift can be accordingly adjusted to 360°/p, where *(p)* represents the total number of interleaved buck converter phases [18].

Circuit averaging is performed to replace the switches with their average model. However, in practical conditions, each phase contains two switching devices containing on-state resistance and an inductor with an inductor series with resistance. The equivalent of the series resistance (ESR) in each phase is in Eq. (1) [19, 20].

$$R_{sp} = R_{swp} + R_{Lp}, p = 1, 2, 3 \tag{1}$$

where R_{sp} is total converter resistance characteristic in each converter phase that consists of switching device resistance R_{swp} and inductor internal resistance R_{Lp}.

Eq (1) is assumed as the parasitic capacitor C_o resistance is minimal and shared with each phase, which could be neglected. A continuous DC input voltage source supplies IBC to simplify the analysis process. The L_1, L_2, and L_3 values are equal and will be denoted as L_s. Utilizing KCL and looking at Figure 2, the charging current i_o is described as the total amount of inductor current $i_L(t)$ in each phase determined as Eq. (3) for calculating the total amount of current during a period or Eq. 4 to calculate the charging current at a specific time [18, 19, 21].

$$i_o(t) = \sum_p i_L(t) \approx i_o \tag{2}$$

$$i_o = i_{L1} + i_{L2} + i_{L3} \tag{3}$$

Eq. (2) can be derived to prescribe the charging voltage v_o as Eq. (4).

$$v_o = i_o \frac{r}{rC_o + 1} \tag{4}$$

where r is the battery's internal resistance, and C_o is the DC–DC output capacitor.

Each IBC phase constantly shifted at 120° among itself. The peak output current ripple in a complete span duty cycle for each phase $d_1(t)$, $d_2(t)$, $d_3(t) \in [0, 1]$ written as Eq. (5) [22].

$$\Delta i_o\left(d_p\left(t\right)\right) = \frac{V_{Co}}{2L_s f_{sw}}\left(d_p\left(t\right) - \frac{k-1}{p}\right) \cdot \left(1 - p\left(d_p\left(t\right) - \frac{k-1}{p}\right)\right) \quad (5)$$

Eq (5) is used for the following conditions: $\frac{k-1}{p} \leq d_t\left(s\right) \leq k/p$, where $k = 1, \ldots, p$, f_{sw} is frequency switching, V_{Co} is the voltage at the capacitor output filter, and $d_p\left(t\right)$ represents the duty cycle in one of the converter phases at a given time.

The IBC topology significantly mitigates inductor current ripple through its inherent ripple cancellation feature [23]. Increasing the number of phases within the IBC can effectively decrease the peak value of the current ripple output. Phase segmentation reduces the inductor value within the converter, thereby preventing degradation in the response stability of the converter, which can occur due to the energy charging and discharging cycles in a large inductor [24]. Furthermore, as illustrated in Eq. (6), the theoretical framework indicates that the output current ripple of the IBC can approach zero by augmenting the number of phases. This characteristic is particularly beneficial in designing and implementing high-performance fast charger topologies intended for supplying large currents to batteries. The correlation between the maximum output current ratio and the maximum inductor current ripple within the IBC is quantitatively described in Eq. (6).

$$r = \frac{\max(\Delta i_{ou} d_p\left(t\right))}{\max(\Delta i_L d_p\left(t\right))} = \frac{1}{p} \quad (6)$$

where $\Delta i_L d_p\left(t\right)$ is the inductor current written as Eq. (7)

$$\Delta i_L\left(d_p\left(t\right)\right) = \frac{v_o}{2L_s f_{sw}} d_p\left(t\right)\left(1 - d_p\left(t\right)\right) \quad (7)$$

The proposed IBC topology also incurs power losses in practical conditions, as mentioned in [23].

The power losses in the IBC are derived from the resistance equation in the converter in Eq. (1), represented as Eq. (8).

$$P_{loss} = P_c + P_{sw} \quad (8)$$

Where P_c is conduction losses $P_c = I_{rms}\ x\ R_{ON}$ with I_{RMS} as charging current root mean square (RMS) flowing through the switching device and R_{ON} is the switch's on-state resistance. P_{sw} stands for switching losses $P_{sw} = 0.5 \times V_D \times i_o \times \left(t_{don} + t_r + t_{doff} + t_f\right) \times f_{sw}$ with V_D as drain voltage, t_r as the switching device rise time t_{don} and t_{doff} is the time delay during the on and off periods, respectively.

3. Battery Parametric Model

The battery-selected model was initially developed in [25]. A detailed explanation and definition of the battery mathematical modelling can be found in the MATLAB documentation using Eq. (9); the battery open circuit voltage can be measured from the battery equivalent circuit in Figure 2.

$$V_{Bat_{oc}}\left(it, i*, i\right) = E_0 - K \cdot \frac{Q}{it + 0.1} \cdot i - K \cdot \frac{Q}{Q - it} \cdot it + A \cdot \exp\left(-B \cdot it\right) \quad (9)$$

Where E_0 is the nonlinear voltage input, E_0 is the constant voltage input, K is the polarization constant in (V/Ah), Q is the maximum battery capacity (Ah), A is the exponential voltage input, B is the exponential capacity (Ah^{-1}), $i*$ is the low-frequency current dynamic (A), it is the battery current (A), $\exp(s)$ is exponential zone dynamics (V). The SoC, or battery nominal present capacity, is the charge amount. It is 0% when the battery is fully discharged and 100% when fully charged. The Battery SoC in the time (t) is calculated using Eq. (10).

$$SoC(t) = \frac{Q\ i(t)}{Q}\ .\ 100\% \quad (10)$$

4. The Proposed Intelligent Control

The battery was in charging mode when the battery current exceeded zero $(i^* < 0)$, and the battery open circuit voltage, as shown in Eq. (10). To fulfil the proposed fast charging scenario for E2W batteries, the

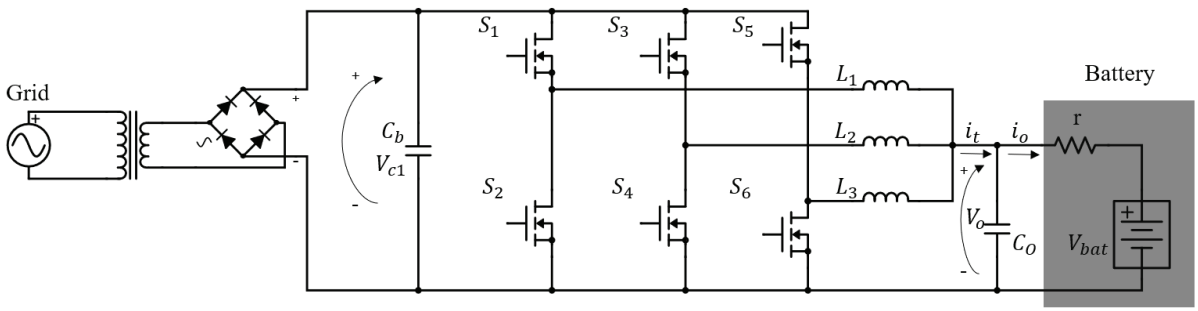

Figure 2. Proposed charger architecture

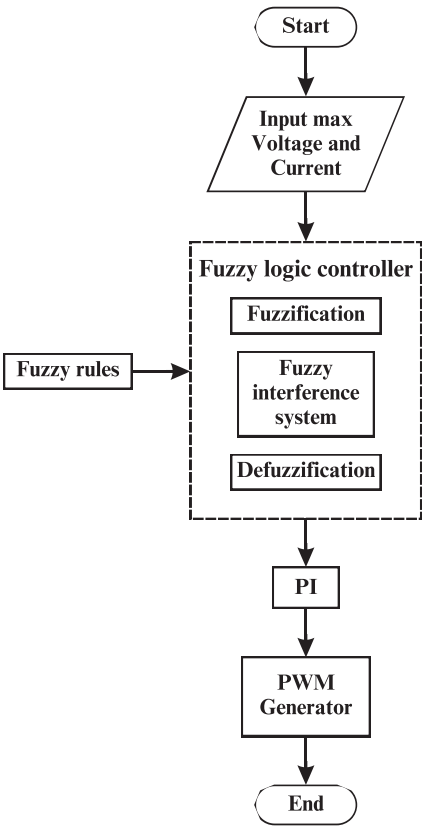

Figure 3. Charging Algorithm

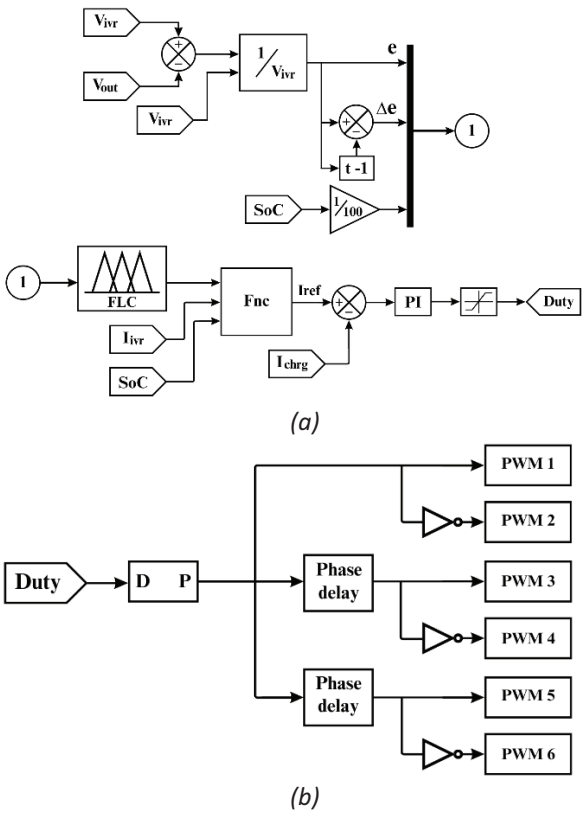

Figure 4. (a) Charging control block, (b) PWM generator

PI-FLC algorithm ensures that the system meets different charging standards for each E2W battery.

In contrast with the conventional CC–CV method, which prioritizes rapid charging solely during the 0–80% SoC range. As depicted in Figure 3, this work implements adaptive current profiling charging to mitigate exorbitant charging currents in low SoC (0–20%) and overvoltage risks in high SoC (80–100%). The three-stage charging protocol operates as follows: (a) normal-rate charging (0-0.8 C) at 0–20% SoC to prevent exorbitant charging current from damaging the battery; (b) accelerated charging (0.8-1 C) at 20–80% SoC to minimize the duration; and (c) tapered charging (0-0.5 C) at 80–100% SoC to avoid battery damage due to extensive charging current.

Figure 4 illustrates the output of FLC, which is a reference C-rate. This C-rate is then multiplied by the battery capacity I_{ivr} to establish the reference charging current value. This reference current is successfully compared with the measured current to generate a current error, which will be the PI control input. The PI control calculates the appropriate duty cycle to achieve the desired reference current and voltage. Furthermore, the PI-FLC hybrid controller dynamically resolves nonlinear battery dynamics by combining PI-based voltage regulation with FLC-driven multi-constraint optimization.

Charging parameters are fuzzified into membership functions, enabling the FLC to autonomously select charging modes through 75 rule-based decisions. This dual-loop architecture compensates for PI controllers' inherent limitations in adaptive charging parameters under battery nonlinear characteristics.

The PI controller used in the proposed method is conventional PI, where $PI = K_P + K_I 1/s$ which is designed to obtain a monotonic response. In particular, the values of $K_p = 0.75$ and $K_I = 50$, respectively, and the PI output is limited with the saturation value of 0-0,97. As depicted in Figure 5, the FLC algorithm had three membership inputs membership function: error voltage described as $\mu_e = (V_{ivr} - V_O)/\ V_{ivr} \in [-1\ 1]$ where V_{ivr} is the battery voltage set point at charging mode, delta error is differential between measured μ_e and μ_e at t-1 described as $\mu_{\Delta e} = \mu_e - \mu_e(t-1) \in [-1\ 1]$, and battery SoC is described as $\mu_{SoC} = SoC(t)/100) \in [0\ 1]$ fuzzy membership output is the reference C-rate $\mu_{i_{ivr}} \in [0\ 1]$.

Table 1 illustrates the normal rate charging conditions in which the current and voltage rise exponentially toward the battery charging voltage and maximum charging capacity. Table 2 illustrates the accelerated charging condition securing the maximum charging current and voltage. Table 3 illustrates the tapered charging condition where the current drops slowly from the maximum charging current to zero when the battery SoC reaches 100% and maintains the set point charging voltage.

5. Results and Discussion

The proposed system was validated using MATLAB/Simulink and simulated based on the charger

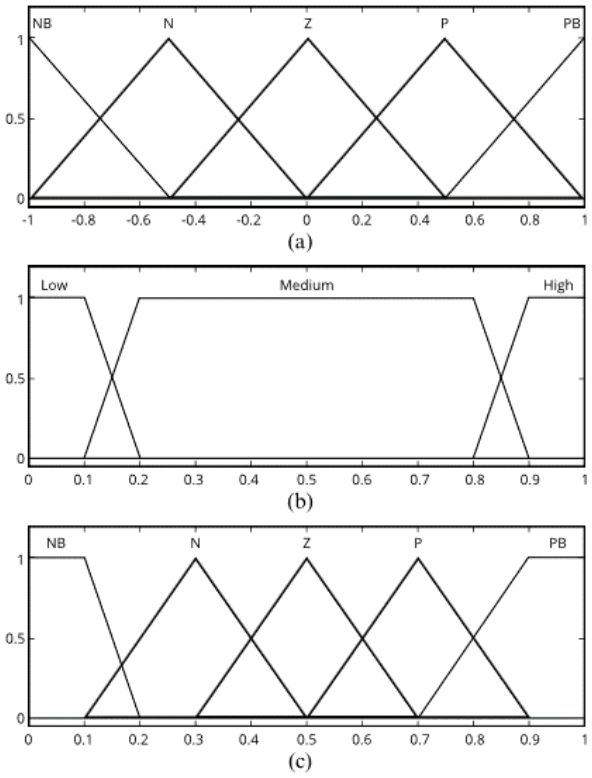

Figure 5. Fuzzy membership function (a) input error and Δerror, (b) input SoC, (c) Output

Table 1. The fuzzy rule for low SoC level

SoC: Low		error				
		NB	**N**	**Z**	**P**	**PB**
Δ error	**NB**	Z	Z	Z	Z	Z
	N	Z	N	N	Z	P
	Z	Z	Z	Z	P	PB
	P	Z	Z	P	PB	PB
	PB	Z	P	PB	PB	PB

Table 2. The fuzzy rule for medium SoC level

SoC: Medium		error				
		NB	**N**	**Z**	**P**	**PB**
Δ error	**NB**	PB	PB	PB	PB	PB
	N	PB	PB	PB	PB	PB
	Z	PB	PB	PB	PB	PB
	P	PB	PB	PB	PB	PB
	PB	PB	PB	PB	PB	PB

Table 3. The fuzzy rule for high SoC level

SoC: High		error				
		NB	**N**	**Z**	**P**	**PB**
Δ error	**NB**	NB	NB	NB	NB	NB
	N	NB	NB	NB	NB	N
	Z	NB	NB	NB	NB	N
	P	NB	NB	NB	N	N
	PB	NB	NB	N	N	N

parameters outlined in Table 4. Furthermore, the proposed charging topology has also been validated by hardware implementation.

Table 4. The charger simulation parameters

Parameter	**Value**
RMS Input Voltage	220-230V 50Hz (AC)
AC Transformator	1:2
Rectifier	2 kW
Switching device	MOSFET N-type Rd = 0.01 Ω Rs = 1e5 Ω
Inductor L_s	1e-3H
Capacitor output C_O	200e-6F
Voltage output V_o	48-84V
Output current i_o	0-20A

5.1. Simulation Implementation Result

The proposed system was developed using MATLAB/Simulink, incorporating charger parameters delineated in Table 4. A nickel-manganese-cobalt (NMC) battery [25], configured in a 20s8p topology (nominal voltage of 72 V and a capacity of 20.4 Ah), was utilized for testing purposes. Comparative analyses were conducted against the PID CC-CV and PI CC algorithms. These assessments evaluated charging current and voltage dynamics, transient response, and total charging duration to ensure a rigorous and unbiased performance validation.

Figure 6 demonstrates the transient voltage response to an 84 V setpoint. The proposed method effectively achieves voltage stabilization within 1.25 ms, exhibiting a response time twice as rapid as the PID CC–CV algorithm, which stabilizes at 2.5 ms. In contrast, the PI-CV method fails to reach convergence, displaying a steady-state error of 2.3%. These results underscore the superior transient response of the proposed method.

Table 5 illustrates that the current regulation performance across the entire SoC range is quantitatively assessed. The proposed system maintains a current deviation of ± 4 A at 20% SoC while operating at a 1 C-rate (20.4 A) during the accelerated charging phase. Furthermore, the current throttling rate is 0-0.8 C-rate and 0-0.5 C-rate at 0% and 80% SoC, respectively. As depicted in Figure 7, the proposed method effectively mitigates risks associated with battery thermal run and cell damage. The system achieves current tapering to 0 A at 100% SoC.

Charging time comparisons presented in Figure 7 reveal that the PI-FLC algorithm accomplishes a 0 to 100% SoC charging duration of 57.75 minutes. This achievement represents a significant reduction of 67.9% and 75.9% compared to the PID CC-CV (180 min) and PI-CV (240 min) methods, respectively. The performance of the proposed system exceeds that of traditional PID CC-CV chargers currently implemented in commercial E2W systems [26], thus demonstrating its viability for industrial applications.

5.2. Hardware Implementation Result

The proposed hardware implementation of the 3Phase IBC-based charger was developed to validate theoretical performance metrics and demonstrate

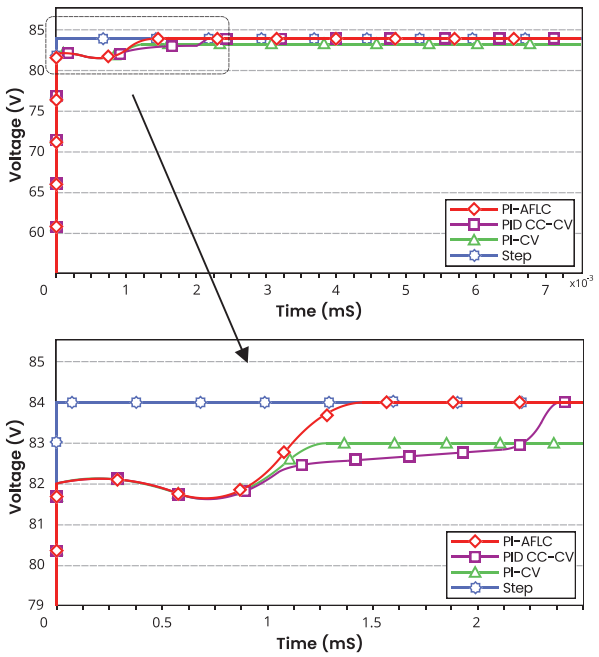

Figure 6. The comparison of charging voltage characteristics

Table 5. The charging current characteristics of the proposed algorithm

SoC (%)	Peak Current (A)	Average Charging Current (A)	C-Rate	Charging Voltage (V)
0	13	10	0.5	84
20	24	20	1	84
40	23	20	1	84
60	22	20	1	84
80	15	10	0.5	84
100	0	0	0	84

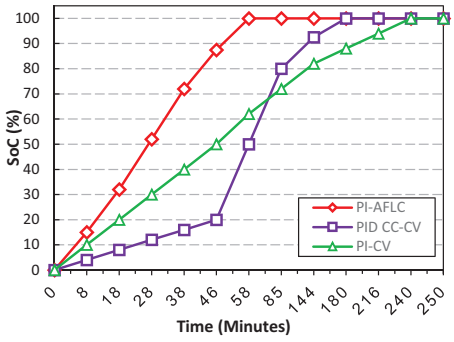

Figure 7. Charging time performance

practical applicability for E2W systems. The experimental setup encompasses modular architecture featuring an AC-DC rectification stage, a 3Phase IBC, precision sensing modules for real-time voltage and current monitoring, and a microcontroller unit (MCU) executing a hybrid PI-FLC algorithm. Operating from a standard 220–230 V AC (50 Hz) input, the system rectifies to a 30 V DC bus and delivers a regulated 21 V DC output to charge a 5-series, 1-parallel (5S1P) lithium-ion battery array.

Table 6. The charger hardware implementation parameters

Parameter	Value
RMS Input Voltage	220-230V 50Hz (AC)
Voltage Input	30 V
Current Input	0.4 A
Power Input	12 W
Voltage Output	21 V
Current Output	0.564 A
Output Capacitor	100 uF
Inductor	60 uH
Switching Device	MOSFET
Switching Frequency	30 kHz
Battery Array	5 series 1 parallel
Power Output	11.85 W
Charger Efficiency	98.8 %

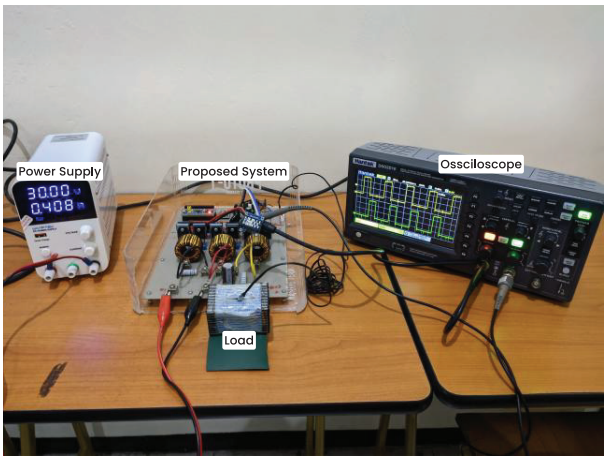

Figure 8. Hardware experimental setup

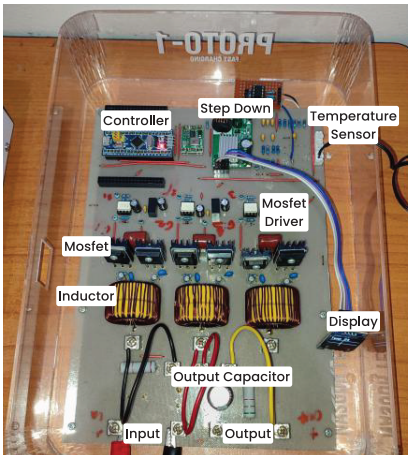

Figure 9. Hardware implementation of the proposed charging topology

The experimental setup is illustrated in Figure 8. The hardware parameters outlined in Table 6 demonstrate an input power of 12 W (30 V, 0.4 A), yielding an output of 11.85 W (21 V, 0.564 A) and achieving an exceptional efficiency of 98.8%. This performance is attributed to the low on-resistance of the MOSFETs, high-frequency operation at 30 kHz, minimizing core losses in the 60 µH inductor, and reduced ripple current enabled by the 100 µF output capacitor.

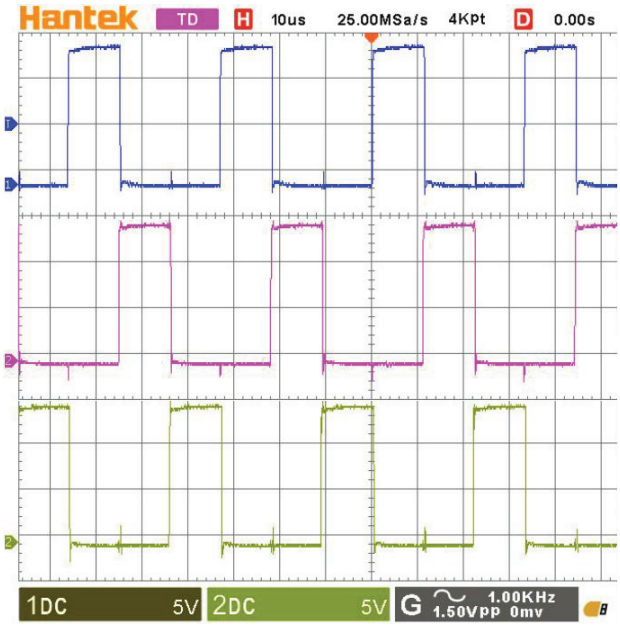

Figure 10. Three phases interleaved PWM signal result 30Khz

Figure 9 provides a granular view of hardware realization, highlighting the three-phase interleaved PWM signals generated by the MCU. The interleaved operation at 30 kHz ensures continuous input current, minimizes input/output voltage ripple, and distributes thermal stress evenly across the three phases. This configuration enhances power density and mitigates electromagnetic interference (EMI). The stable PWM waveform alignment with the control algorithm's dynamic adjustments confirms the robustness of the PI-FLC in adapting to real-time battery SoC and voltage fluctuations.

Figure 10 depicts the steady-state input voltage waveform, which remains consistently regulated at 30 V DC despite variations in load conditions. This stability is critical for maintaining the integrity of the AC-DC rectification stage and ensuring reliable power delivery to the IBC. Meanwhile, Figure 11 illustrates the output voltage waveform, showcasing the charger's ability to maintain a precise 21 V DC under dynamic loading. Notably, the absence of significant overshoot or oscillations during transient responses validates the hybrid PI-FLC algorithm's effectiveness in enforcing tight voltage and current thresholds, even during rapid SoC changes. The interleaved architecture and optimized LC filter achieve minimal voltage ripple at the output.

Charging efficiency (η) and charging time (t) are critical metrics in EV charging systems. Efficiency quantifies power conversion effectiveness while charging time reflects the system's ability to deliver energy rapidly. This study compares recent converter topologies and control algorithms, proposing a novel 3-phase IBC with PI-FLC for enhanced performance. The charging efficiency is described in (11)

$$\eta = \frac{P_{chrg}}{P_{in}} \cdot 100\% \tag{11}$$

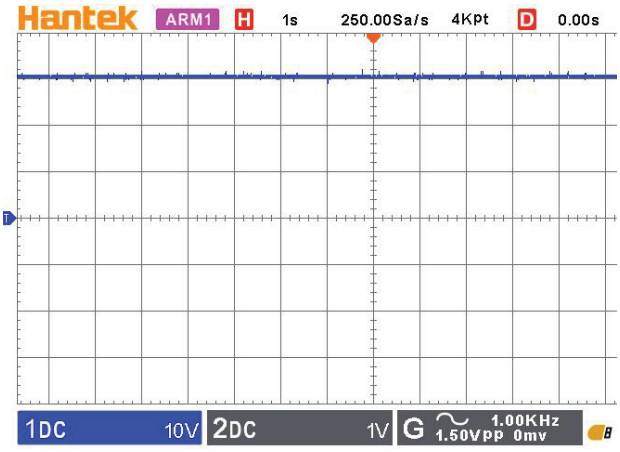

Figure 11. Charger input voltage

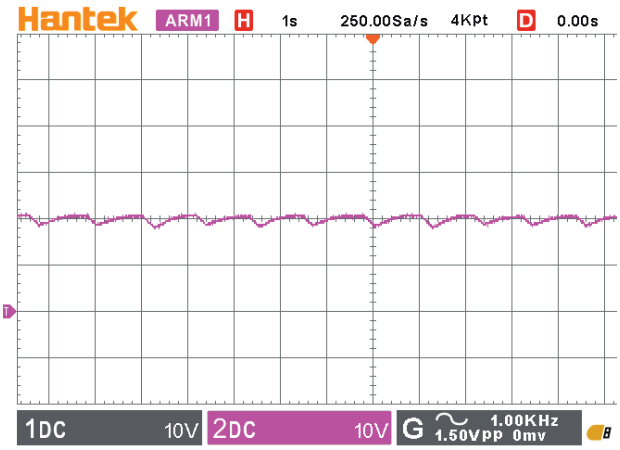

Figure 12. Charger output voltage

Where P_{chrg} is the charging power and P_{in} is the charger input power. Charging time from 0% to 100% SoC depends on battery energy capacity (E_{bat}) and effective charging power ($P_{chrg} \times \eta$) mathematically modelled as (12).

$$t = \frac{E_{bat}}{P_{chrg}\,\eta} \cdot 60(\text{min}) \tag{12}$$

Eq. (11) and (12) are then used to calculate the efficiency and charging speed of the charger in various previous methods which are then included in Table 7. This table presents a comparison between the previous charging methods and the proposed method, proving the efficacy of the proposed method.

Table 7 compares various power converters and control algorithms in EV charging systems from 2020 to 2025. Various converters from previous studies were compared to evaluate their performance in charging batteries. The use of diverse algorithms resulted in variations in charging efficiency. The battery specifications are sometimes different, by calculating the charging time using Eq. (12), although each algorithm is tested using different battery specifications, Eq. 12 will provide the same charging time value according to the performance and capacity of the charger. Efficiency ranges from 92.3% to 98.8%, with charging times between 65 and 175 minutes.

Table 7. Comparison between the proposed method and previous methods

Ref.	Year	Converter Type	Algorithm	Efficiency (%)	Charging Time 0-100% SoC (min)
[27]	2012	Boost	Neural Network	97.8	85
[28]	2018	Flyback	PSO	94.2	100
[29]	2019	Quasi-Resonant	Hysteresis Control	97.5	70
[15]	2020	Cuk	DCM	-	120
[30]	2020	Buck-Boost	FLC	95.5	90
[31]	2021	SEPIC	PID	92.3	110
[32]	2022	Interleaved Boost	FLC	98.5	65
[17]	2023	Buck	ANFIS	-	175
[33]	2023	Zeta	Sliding Mode Control	98.1	80
[34]	2024	LLC	GA	96.7	95
[35]	2024	Dual Active Bridge	MPC	97.9	75
Proposed	2025	3-Phase IBC	PI-FLC	**98.8**	**57.75**

The leading model for 2025, the 3-Phase Interleaved Boost Converter (IBC) with PI-FLC, achieves 98.8% efficiency and the fastest charging time of 57.75 minutes, demonstrating the advantages of the interleaved topology with PI-FLC.

6. Conclusion

The proposed high-performance fast charger for E2W, utilizing a 3 Phase IBC controlled with PI-FLC algorithm, significantly enhances charging efficiency and speed. The PI-FLC optimizes charging current and voltage dynamically by integrating real-time battery current, voltage, and SoC data. Achieving fast charging of 57.75 minutes for a 72 V 20 Ah NMC battery, this system demonstrates a 67.9% and 75.9% reduction in charging time compared to PID CC-CV (180 min) and PI-CV (240 min), respectively. Moreover, the proposed method outperforms several cutting-edge charging methods, such as a Zeta converter with SMC with 98.1% efficiency and 80 min charging time, Quasi-Resonant converters with hysteresis control with 97.5% efficiency and 70 min charging time, Interleaved Boost with FLC 98.5% efficiency and 65 min charging time, and Dual Active Bridge with MPC 97.9% efficiency and 75 min charging time. The hardware implementation demonstrated 98.8% efficiency during testing at a 0.22 C rate. The 3-phase IBC topology minimizes output current ripple and EMI, while the adaptable PI-FLC algorithm prevents overcharging by precisely regulating voltage and current. By addressing the balance between rapid charging requirements and battery longevity, this innovation presents a scalable, effective, and safe solution for the evolving demands of the E2W ecosystem, ultimately contributing to the sustainability of electric mobility.

AUTHORS

Subiyanto – Department of Electrical Engineering, Universitas Negeri Semarang, Semarang, 50229, Indonesia, e-mail: subiyanto@mail.unnes.ac.id.

Rizky Ajie Aprilianto* – Department of Electrical Engineering, Universitas Negeri Semarang, Semarang, 50229, Indonesia, e-mail: rizkyajiea@mail.unnes.ac.id.

Mario Norman Syah – Department of Electrical Engineering, Universitas Negeri Semarang, Semarang, 50229, Indonesia, e-mail: marionormansyah@mail.unnes.ac.id.

Bagaskoro Saputro – Department of Electrical Engineering, Universitas Negeri Semarang, Semarang, 50229, Indonesia, e-mail: bagaskoro.s@mail.unnes.ac.id.

Abdurrakhman Hamid Al-Azhari – Department of Electrical Engineering, Universitas Negeri Semarang, Semarang, 50229, Indonesia, e-mail: abdurrakhmanhamid@mail.unnes.ac.id.

Nektar Cahayasabda – Department of Electrical Engineering, Universitas Negeri Semarang, Semarang, 50229, Indonesia, e-mail: nektarcahayasabda@gmail.com.

Bayu Adi Pambudi – Department of Electrical Engineering, Universitas Negeri Semarang, Semarang, 50229, Indonesia, e-mail: bayuadipambudi@gmail.com.

Faiq Mananul Faqih – Department of Electrical Engineering, Universitas Negeri Semarang, Semarang, 50229, Indonesia, e-mail: faiqmanal77@gmail.com.

Icha Arifah Annisa – Department of Electrical Engineering, Universitas Negeri Semarang, Semarang, 50229, Indonesia, e-mail: ichaarifah03@gmail.com.

Dwi Bagas Nugroho – Department of Electrical Engineering, Universitas Negeri Semarang, Semarang, 50229, Indonesia, e-mail: dwibagasn@gmail.com.

Siva Khaaifina Rachmat – Department of Electrical Engineering, Universitas Negeri Semarang, Semarang, 50229, Indonesia, e-mail: sivaakhaaifina@gmail.com.

Dewi Anggriani – Department of Electrical Engineering, Universitas Negeri Semarang, Semarang, 50229, Indonesia, e-mail: dewianggriani480@gmail.com.

*Corresponding author

References

[1] H. Tu et al., "Extreme Fast Charging of Electric Vehicles: A Technology Overview," *IEEE Transactions on Transportation Electrification*, vol. 5, no. 4, 2019, pp. 861–878; doi: 10.1109/TTE.2019.2958709.

[2] A. Ghosh, "Possibilities and Challenges for the inclusion of the Electric Vehicle (EV) to Reduce the Carbon Footprint in the Transport Sector: A Review," *Energies (Basel)*, vol. 13, no. 10, 2020, pp. 1–2; doi: 10.3390/en13102602.

[3] M. Bharathidasan, V. Indragandhi, and B. Aljafari, "Hybrid Controlled Multi-Input DC/DC Converter for Electric Vehicle Application," *International Transactions on Electrical Energy Systems*, vol. 2023, pp. 1–16; doi: 10.1155/2023/8308418.

[4] D.N. Huu and V.N. Ngoc, "A Three-Stage of Charging Power Allocation for Electric Two-Wheeler Charging Stations," *IEEE Access*, vol. 10, 2022, pp. 61080–61093; doi: 10.1109/ACCESS.2022.3181731.

[5] I. Veza et al., "Electric Vehicles in Malaysia and Indonesia: Opportunities and Challenges," *Energies (Basel)*, vol. 15, no. 7, 2022, pp. 1–4; doi: 10.3390/en15072564.

[6] R. Swapnil and V.N. Kalkhambkar, "Optimal Operation Model of Vehicle to Vehicle Charging System," *Journal of Electrical and Electronics Engineering*, vol. 15, no. 1, 2022, pp. 52–58; https://www.proquest.com/openview/6abce8708f539109954a48200386c0ae/1?pq-origsite=gscholar&cbl=54417

[7] P. Sharma et al., "A Comprehensive Study on Electrical Vehicle in Charging Infrastructure, Challenges and Future Scope," *Electric Vehicles, Green Energy and Technology*, N. Patel et al., eds., Springer, 2021, pp. 1–285; doi: 10.1007/978-981-15-9251-5_16.

[8] P. Sharma, A. Kumar Sharma, and A.K. Vyas, "Comparative Study of DC-DC Converter With Different Control Techniques," *Recent Advances in Renewable Energy Sources*, P. Sharma, ed., RARES2021, 2021, pp. 1–6; doi: https://papers.ssrn.com/sol3/papers.cfm?abstract_id=3808564#

[9] F. Mumtaz et al., "Review on Non-isolated DC-DC Converters and their Control Techniques for Renewable Energy Applications," *Ain Shams University*, 2021; doi: 10.1016/j.asej.2021.03.022.

[10] J. Anzola et al., "Review of Architectures Based on Partial Power Processing for DC-DC Applications," *Institute of Electrical and Electronics Engineers Inc*, 2020; doi: 10.1109/ACCESS.2020.2999062.

[11] H. Ye et al., "High Step-Up Interleaved dc/dc Converter with High Efficiency," *Energy Sources, Part A: Recovery, Utilization and Environmental Effects*, vol. 46, 2020, pp. 4886–4905; doi: 10.1080/15567036.2020.1716111.

[12] P. Sharma, D.K. Dhaked, and A.K. Sharma, "Mathematical Modeling and Simulation of DC-DC Converters Using State-Space Approach," *Proceedings of Second International Conference*, J.C. Bansal, K. Deep, and A.K. Nagar, eds., Springer, 2020, pp. 1–737; doi: 10.1007/978-981-15-6707-0.

[13] P. Sharma et al., "Coati Optimized FOPID Controller for Non-Isolated DC–DC Converters in EV Charging Application," *IET Power Electronics*, 2024, pp. 2771–2784; doi: 10.1049/pel2.12798.

[14] P. Sharma et al., "Novel Current-Fed Bidirectional DC-DC Converter for Battery Charging in Electric Vehicle Applications with Reduced Spikes," *Electricity*, vol. 5, no. 4, 2024, pp. 1022–1048; doi: 10.3390/electricity5040052.

[15] K. Shreya et al., "CUK Converter Fed Resonant LLC Converter Based Electric Bike Fast Charger for Efficient cc/cv Charging Colution," *Journal of Applied Science and Engineering*, vol. 24, no. 3, 2020, pp. 331–338; doi: 10.6180/jase.202106_24(3).0008.

[16] Y.-S. Cheng et al., "Design and Implementation of Li-ion Battery Charger Using State-of-Charge Estimation with Fuzzy Temperature Control," in *2015 IEEE ICIT*, 2015, p. 799; doi: 10.1109/ICIT.2015.7125402.

[17] S.S. Hussein, A.J. Abid, and A.A. Obed, "ANFIS-Based New Approach for an Optimal Lithium-Ion Battery Charging Control," in *2023 IEEE 3rd International Conference in Power Engineering Applications: Shaping Sustainability Through Power Engineering Innovation, ICPEA 2023*, 2023, pp. 248–251; doi: 10.1109/ICPEA56918.2023.10093226.

[18] G. Balen et al., "Modeling and Control of Interleaved Buck Converter for Electric Vehicle Fast Chargers," in *2017 COBEP*, 2018, pp. 1–6; doi: 10.1109/COBEP.2017.8257412.

[19] L. Ntogramatzidis et al., "A Novel MIMO Control for Interleaved Buck Converters in EV DC Fast Charging Applications," *IEEE Transactions on Control Systems Technology*, vol. 31, no. 4, 2023, pp. 1892–1900; doi: 10.1109/TCST.2023.3237497.

[20] M. Carbajal-Retana et al., "Interleaved Buck Converter for Inductive Wireless Power Transfer in dc–dc Converters," *Electronics (Switzerland)*, vol. 9, no. 6, pp. 1–15; doi: 10.3390/electronics9060949.

[21] S. Cuoghi et al., "Multileg Interleaved Buck Converter for EV Charging: Discrete-Time Model and Direct Control Design," *Energies (Basel)*, vol. 13, no. 2, pp. 1–8; doi: 10.3390/en13020466.

[22] A. Garg and M. Das, "High Efficiency Three Phase Interleaved Buck Converter for Fast Charging of EV," in *ICPEE 2021 - 2021 1st International Conference on Power Electronics and Energy*, 2021, pp. 1–5; doi: 10.1109/ICPEE50452.2021.9358486.

[23] K. Drobnic et al., "An Output Ripple-Free Fast Charger for Electric Vehicles Based on Grid-Tied

Modular Three-Phase Interleaved Converters," *IEEE Trans Ind Appl*, vol. 55, no. 6, 2019, pp. 6102–6114; doi: 10.1109/TIA.2019.2934082.

[24] Y.T. Yau, K.I. Hwu, and J.J. Shieh, "Minimization of Output Voltage Ripple of Two-Phase Interleaved Buck Converter with Active Clamp," *Energies (Basel)*, vol. 14, no. 16, 2021, pp. 1–30; doi: 10.3390/en14165215.

[25] A.I. Pózna, K.M. Hangos, and A. Magyar, "Design of Experiments for Battery Aging Estimation," *IFAC-PapersOnLine*, 2018, pp. 386–391; doi: 10.1016/j.ifacol.2018.11.733.

[26] H. Li et al., "Cooperative CC-CV Charging of Supercapacitors Using Multicharger Systems," *IEEE Transactions on Industrial Electronics*, vol. 67, no. 12, 2020, pp. 10497–10508; doi: 10.1109/TIE.2019.2962485.

[27] L. Gan, U. Topcu, and S.H. Low, "Optimal Decentralized Protocol for Electric Vehicle Charging," *IEEE Transactions on Power Systems*, vol. 28, no. 2, 2012, pp. 940–951; doi: 10.1109/TPWRS.2012.2210288.

[28] M.C. Kisacikoglu, F. Erden, and N. Erdogan, "Distributed Control of PEV Charging Based on Energy Demand Forecast," *IEEE Trans Industr Inform*, vol. 14, no. 1, 2018, pp. 332–341; doi: 10.1109/TII.2017.2705075.

[29] S. Bhatnagar et al., "Charging System Analysis in Static and Dynamic Wireless Electric Vehicle," *International Journal of Advanced Research in Engineering and Technology (IJARET)*, vol. 10, no. 1, 2019, pp. 104–120; doi: https://www.doi.org/10.34218/IJARET.10.1.2019.011

[30] G. Madhur et al., "Fast Charging Electric Vehicle using Fuzzy Logic Controller," *International Journal of Engineering Research & Technology (IJERT)*, vol. 9, pp. 499–502; doi: 10.17577/IJERTV9IS050426.

[31] D.N. Huu and V.N. Ngoc, "Analysis Study of Current Transportation Status in Vietnam's Urban Traffic and the Transition to Electric Two-Wheelers Mobility," *Sustainability (Switzerland)*, vol. 13, no. 10, 2021, pp. 1–27; doi: 10.3390/su13105577.

[32] T. Saravanakumar and R.S. Kumar, "Fuzzy Based Interleaved Step-up Converter for Electric Vehicle," *Intelligent Automation and Soft Computing*, vol. 35, no. 1, 2022, pp. 1103–1118; doi: 10.32604/iasc.2023.025511.

[33] D.V. Pendam and T.M. Rofin, "Electric Vehicle and Charging Infrastructure Development: A Comprehensives Review Using Science Mapping and Thematic Analysis," 2023; doi: 10.1007/978-981-99-1019-9_26.

[34] V. N. Ngoc and D. N. Huu, "Optimal Valley-Filling Algorithm for Electric Two-wheeler Charging Stations," *Engineering, Technology and Applied Science Research*, vol. 14, no. 1, pp. 13072–13077, 2024; doi: 10.48084/etasr.6569.

[35] Z. Chen, Z. Zheng, X. Tang, and Y. Wu, "Model Predictive Controlled Dual Active Bridge Converter with Efficiency Optimization and Fast Dynamic Response," *Journal of Electrical Engineering and Technology*, vol. 19, no. 1, 2024; doi: 10.1007/s42835-023-01569-x.